European Journal of Nuclear Medicine and Molecular Imaging (2019) 46:2558–2568
https://doi.org/10.1007/s00259-019-04443-z

ORIGINAL ARTICLE

Anatomical localization of radiocolloid tracer deposition affects outcome of sentinel node procedures in prostate cancer

C. M. de Korne[1,2] · E. M. Wit[2] · J. de Jong[3] · R. A. Valdés Olmos[1,4] · T. Buckle[1,2] · F. W. B. van Leeuwen[1,2] · H. G. van der Poel[2]

Received: 29 May 2019 / Accepted: 16 July 2019 / Published online: 3 August 2019

Abstract

Purpose Diagnostic imaging modalities have moderate sensitivity for the identification of lymph node (LN) metastases in prostate cancer (PCa) patients. Mapping the lymphatic drainage from the prostate can help to identify the LNs directly draining from the tumour (sentinel nodes (SNs)); the LNs stated to have the highest chance of containing metastatic cancer cells. Although the lymphatic drainage may differ between segments within the prostate, the location of the primary tumour is not routinely taken into account during peripheral zone-aimed tracer administration. This study evaluates whether linking the SN procedure to the primary cancer deposits increases the identification accuracy of lymphatic metastases.

Methods Sixty-seven PCa patients, scheduled for robot-assisted laparoscopic prostatectomy (RALP) and extended lymph node dissection (ePLND) with subsequent SN biopsy, were included in this retrospective study. After injection of the hybrid tracer ICG-^{99m}Tc-nanocolloid in the prostate, SN mapping was performed based on lymphoscintigraphy and SPECT/CT. SNs were resected using a combination of radio- and fluorescence guidance. Pathology was used to determine the primary tumour location and metastatic spread. Fluorescence imaging of paraffin-embedded prostate tissue was used to determine the location of the tracer deposits in the prostate. This deposition was related to the primary tumour location, the lymphatic drainage pattern of the injected tracer, and the metastatic spread.

Results In total 265 radioactive LNs (211 SNs and 54 higher-echelon nodes in 64 patients; 4.3 LNs per patient; IQR: 2–6) were identified. In three patients (4%) preoperative imaging did not allow identification of SNs. Tumour-positive SN visualization within the pelvis was shown to be influenced by intraprostatic location of tracer administration. This could be concluded from (1) a clear correlation between lymphatic drainage to the right or left side of the body and tracer deposition on the right or left side of the prostate, (2) visualization of a higher number of LNs after dorsal tracer deposition compared with ventral tracer deposition, (3) different drainage patterns observed for tracer deposition into the base or apex of the prostate, and (4) the indication that intratumoural tracer deposition increases the chance of visualizing nodal metastases compared with extratumoural tracer deposition.

Conclusions The correlation between the location of the tracer deposits, the location of the primary tumour, and the visualization of the (tumour-positive) SNs indicated that placement of tracer deposits is of influence on the visualized lymphatic drainage pattern. This suggests that tracer injection near or into the primary tumour site is beneficial for the identification of metastatic spread.

Keywords Prostate cancer · Sentinel (lymph) node · Hybrid tracer · Tracer deposition · Fluorescence-guided surgery · Radio-guided surgery

C. M. de Korne and E. M. Wit contributed equally to this work.

This article is part of the Topical Collection on Oncology – Genitourinary

✉ H. G. van der Poel
h.vd.poel@nki.nl

[1] Interventional Molecular Imaging Laboratory, Department of Radiology, Leiden University Medical Center, Leiden, The Netherlands

[2] Department of Urology, The Netherlands Cancer Institute-Antoni van Leeuwenhoek Hospital, Amsterdam, The Netherlands

[3] Department of Pathology, The Netherlands Cancer Institute-Antoni van Leeuwenhoek Hospital, Amsterdam, The Netherlands

[4] Department of Nuclear Medicine, The Netherlands Cancer Institute-Antoni van Leeuwenhoek Hospital, Amsterdam, The Netherlands

Introduction

Diagnostic imaging modalities such as computed tomography (CT), magnetic resonance imaging (MRI), and prostate-specific membrane antigen positron emission tomography/computed tomography (PSMA PET/CT) have moderate sensitivity for the identification of lymph node (LN) (macro)metastases in prostate cancer (PCa) patients (39–42% for CT and MRI and 40–71% for PSMA PET/CT [1–3]). Therefore, an extended pelvic lymph node dissection (ePLND) is currently recommended for PCa patients with an estimated risk of nodal metastases exceeding 5% according to the updated Briganti nomogram [4]. Unfortunately, an ePLND is not personalized and is associated with an overall complication rate of 20% [5]. This has driven the desire for less invasive and more accurate technologies that help identify lymphatic (micro)metastases [6]. Mapping of the lymphatic flow from the prostate allows for the identification of the LNs directly draining from the tumour, the so-called sentinel nodes (SNs). Reasoning that rogue metastatic tumour cells disseminate based on the lymphatic flow, the SNs represent the part of the lymphatic network that has the highest chance of containing metastatic cancer cells. Nevertheless, studies wherein combined ePLND and SN procedures were performed have indicated that restriction of the intervention to SN dissections would not allow excision of all nodal metastases [7, 8]. In 13–27% of the patients, however, personalized lymphatic mapping was shown to support the identification of LN metastases that have spread beyond the ePLND template [9–11].

Intraoperative lymphatic mapping in prostate cancer can be performed with colloidal particles (radiocolloids) [12], magnetic particles [13] or small organic dyes (indocyanine green or fluorescein) [14–16]. The use of the hybrid tracer ICG-^{99m}Tc-nanocolloid, allows combination of the most favourable properties of a radiocolloid tracer with those of a fluorescent dye (Fig. 1) [17]. With this tracer, most SNs can be identified preoperatively using lymphoscintigraphy and subsequently anatomically localized by means of single-photon emission computed tomography/computed tomography (SPECT/CT) in the respective LN stations (Fig. 1.2). Intraoperatively, the SNs can be identified at the indicated LN stations via real-time gamma tracing and/or fluorescence imaging (Fig. 1.3). Even when the radioactive signal has decayed, the fluorescent component of the hybrid tracer can be detected [18]. This feature allows scrutinization of the ICG-^{99m}Tc-nanocolloid distribution at pathology (Fig. 1.4). Not only can the tracer accumulation in LNs be identified [19], the primary sites of tracer deposition within the prostate can be retrospectively validated [20].

Lymphatic tracer migration from the prostate differs per individual with drainage to different LN stations within the pelvic area [21]. Combined with the heterogeneous distribution of PCa throughout the prostate, this suggests that the tracer deposition within the prostate could well be a key feature in the execution of a successful SN procedure. A previous pilot study in 19 patients indicated that the location of tracer deposition within the prostate influences lymphatic mapping [20]. In this study, placement of tracer deposits in the dorsal half of the prostate yielded a higher number of visualized LNs compared with deposits placed in ventral half. Furthermore, tracer deposition in the mid gland correlated with a higher number of visualized LNs than tracer deposition near the base or apex of the prostate [20]. However, in this initial feasibility study, the relationship between the tracer- and tumour-dissemination was not investigated.

Reasoning that optimization of tracer deposition procedures could improve the accuracy of the SN procedure in prostate cancer, we investigated the relationship between tumour location, the hybrid tracer deposition site and lymphatic drainage to metastasis containing LNs. This was achieved by correlating pre- and post-operative imaging findings with pathological outcome (tumour location and tumour bearing LNs) to the location of the tracer deposits within the prostate determined through evaluation of fluorescence imaging of paraffin-embedded prostate samples (Fig. 1).

Methods

Patient population

The study protocol (N09IGF; NL28143.031.09), with as primary goal the comparison of the SN procedure via ultrasound guided transrectal injection of ICG-^{99m}Tc-nanocolloid, was approved by the local ethics committee of The Netherlands Cancer Institute, Antoni van Leeuwenhoek Hospital. Sixty-seven patients with prostate carcinoma with an increased risk of nodal metastasis of more than 10% according to MSKCC nomogram that were scheduled for robot-assisted laparoscopic prostatectomy (RALP) and extended pelvic lymph node dissection (ePLND) complemented with lymphatic mapping were included in this retrospective study. Informed consent was obtained from all individual participants included in the study.

Tracer preparation

The hybrid tracer ICG-^{99m}Tc-nanocolloid was prepared as previously described [22]. All tracer preparations were performed under the Dutch *Kernenergiewet* (Nuclear Energy Law) and in accordance with the Dutch guidelines for good manufacturing practice (GMP) as well as with the approval of the local pharmacist.

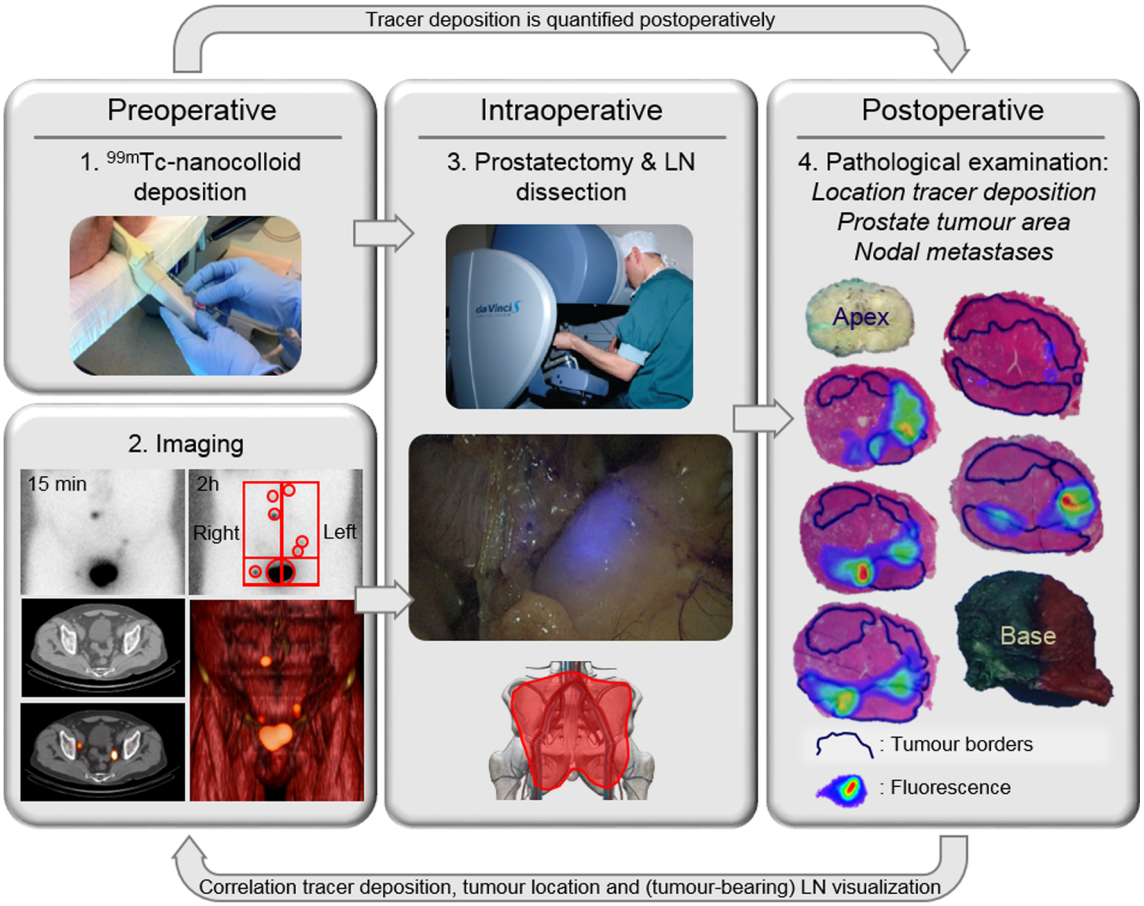

Fig. 1 Study overview. (1–2) Preoperatively, ^{99m}Tc-nanocolloid was deposited in the prostate (1) and the resulting lymphatic drainage was visualized with lymphoscintigraphy (2 top) and SPECT/CT (2 bottom). (3) Intraoperatively, prostatectomy and LN dissection were performed using a four-arm da Vinci S robotic system (top) guided by preoperative images which indicated the draining LN station and intraoperative imaging of the tracer (middle). In addition, an ePLND was performed (bottom). (4) Postoperatively, the location of the tracer deposition, the primary tumour, and the nodal metastases were determined and correlated with the preoperative and intraoperative findings. An overlay between the HE staining and the corresponding fluorescence image of that particular section of the prostate revealed the location of the tracer deposit in relation to the location of the tumour

Tracer deposition

ICG-^{99m}Tc-nanocolloid was administered approximately 4 h prior to surgery. Transrectal positioning of the needle prior to tracer administration was guided by ultrasound (Hitachi, Japan; Fig. 1.1). Four tracer depositions were placed in the prostate aimed at the 0 peripheral zone of the prostate. Both lobes of the prostate were injected with 2 tracer deposits of 0.1 ml each (total volume, 0.4 ml; total dose, ~ 280 MBq). The needle and tubing were flushed with approximately 0.7 ml of saline after placement of each tracer deposit.

Pre-operative imaging

To map the lymphatic drainage planar lymphoscintigraphy was performed at 15 min and 2 h after tracer injection (Symbia T, Siemens; Fig. 1.2). Sentinel nodes (SNs) and higher-echelon nodes (non-SNs) were identified according to previously described procedures [23]. For anatomic localization of the LN stations single photon emission computed tomography with low-dose computed tomography (SPECT/CT) was performed directly after planar lymphoscintigraphy at 2 h using the same camera system (Fig. 1.2). Lymphoscintigrams and SPECT/CT images were analysed using OsiriX medical imaging software (Pixmeo, Switzerland). The quantification of uptake in SNs and non-SNs was based on the lymphoscintigraphy data (Fig. 1.2); the amount of radioactivity in the LNs was determined by measuring the counts/cm^2 per LN. Moreover, the total radioactivity in the prostate lymphatic drainage region was determined by measuring the counts/cm^2 per side of the body (left or right).

Surgical procedure

In the operating room, pre-operatively acquired SPECT/CT images were depicted on a screen where they were used as a roadmap that represents the anatomical location of the

ICG-^{99m}Tc-nanocolloid containing LNs. The surgical intervention was performed using a four-arm da Vinci S robotic system (Intuitive Surgical, USA). At every LN station indicated by SPECT/CT the tracer-positive LNs (SNs and non-SNs) were excised guided by a laparoscopic gamma probe (Europrobe, France) and the Karl Storz fluorescence laparoscope (Karl Storz, Germany). Here, the gamma probe provided the first guidance towards the SN location, whereas the fluorescence laparoscope provided guidance during the last centimetres/mm of the SN identification and actual resection. In addition, an ePLND was performed as described by Klein Jan et al. [22] (Fig. 1.3). During LN dissection, the location of each excised LN was noted. Finally, a prostatectomy was performed. All excised specimens were formalin-fixed and paraffin-embedded to allow further (pathological) assessment.

Quantification of tracer deposition

Following prostatectomy, ex vivo fluorescence imaging of the paraffin-embedded prostate specimens enabled quantification of the tracer distribution per quadrant of the prostate. Fluorescence imaging of paraffin-embedded prostate tissue blocks was used to visualize the location of the tracer injection and its distribution throughout the prostate as previously described [20]. Fluorescence signal intensities were measured using an IVIS 200 camera (Xenogen Corp, USA). For each patient, 3–9 paraffin-embedded tissue sections, together covering the whole prostate from base to apex, were evaluated (Fig. 1.4). Images were acquired with standard ICG filter settings (excitation 745 nm and emission 800 nm) filter settings. Signal intensities (photons/s/cm^2/sr) were quantified using living imaging acquisition and analysis software (Xenogen Corp, USA). To simplify the description of the tracer deposition distribution, the prostate was divided into 4 quadrants (Q1-4) and base vs. apex. Q1 and Q2 representing the right side of the prostate, Q3 and Q4 representing the left side, Q2 and Q3 representing the dorsal and Q1 and Q4 representing the ventral half of the prostate (Fig. 3a). The cranial half of the sections were considered as the base of the prostate and the caudal half of the sections as the apex of the prostate. Per tissue block, the distribution of the fluorescence signal was evaluated by calculating the mean percentage of fluorescence in each quadrant was calculated. The relationship between the location of the tracer injection and the drainage pattern was assessed by correlating the distribution of the tracer injection (left vs. right, dorsal vs. ventral, and base vs. apex) with the location of the tracer-positive lymph nodes. The effect of the location of tracer deposition on lymphatic mapping was investigated by considering three different orientations: left vs. right, dorsal vs. ventral, and base vs. apex (Fig. 3a). The intent during tracer tracer administration was to place the tracer deposits in the peripheral zone of the prostate, equally distributed over the left and right side and the base and apex. Therefore the retrospective analysis of the correlation between the location of tracer deposition and the location of the visualized LNs demanded confinement to the 20% of patients with the most unequal tracer deposition between left vs. right, dorsal vs. ventral, and base vs. apex. To study the left vs. right orientation, the tracer administration side (percentage of fluorescent signal found on the left or right side of the prostate by post-operatively imaging of the paraffin-embedded prostate tissue blocks) was related to the location of the visualized LNs (percentage of LNs found on the left or right side of the body by pre-operatively planar lymphoscintigraphy).

Pathologic examination

Tissue sections of excised lymph nodes and the prostate (base to apex) were stained with haematoxylin and eosin (HE staining). Stained sections were scanned using a slide scanner, where after tumour content/location was delineated by an experienced pathologist. For each prostate section (Q1-Q4), the relative tumour surface (% of total prostate surface) was quantitively calculated using a custom written MATLAB script (version r 2017b, The MathWorks Inc.). An overlay between the HE staining and the corresponding fluorescence image of that particular section of the prostate was used to evaluate the relation between the location of the tumour and the tracer injection site (Fig. 1.4). For tumour-positive LNs, the location of excised LNs was related to the location of the tumour.

Statistical analysis

In earlier data, a lowest median number of 2 SN per patient was recorded [20]. To effectively correlate nodal location with tracer injection location in the prostate an estimated 100 SN would be required. Therefore, at least 50 patients were needed for analysis. To describe variables, the mean and interquartile range (IQR, 25–75%) is provided. To compare two paired or unpaired non-parametric groups of datapoints, respectively the Wilcoxon signed-rank test or the the Mann-Whitney *U* test was used. To measure the linear correlation between different variables, the Pearson correlation was calculated. P values < 0.05 were considered significant. All statistical tests were performed using SPSS Statistics (version 23; IBM Nederland B.V.).

Results

Tracer deposition and preoperative imaging

Lymphoscintigraphy and SPECT/CT allowed preoperative mapping of the lymphatic drainage after intraprostatic tracer injection. Imaging at 2 h supported identification of 265 LNs

in 64 (96%) patients (211 SNs and 54 non-SNs; 4.1 LNs per patient, IQR 2–6). In 3 patients (4%) no SNs were visualised (non-visualization). Quantification of the lymphatic drainage showed non-equally distribution over both sides in the majority of patients ($p = 0.021$; Wilcoxon signed-rank test): in 34 patients (53%), more radioactive LNs were found on the left side, whereas in 21 patients (33%), more LNs were found on the right side. In 9 patients (14%), the same number of LNs was found on both sides.

Intraoperative SN identification

A total of 242 LNs (including SNs and non-SNs) were removed, 17 (found in 16% of the patients) were located in LN stations outside the ePLND template (presacral, preprostatic, umbilical ligament and para-caval region) (Fig. 2b).

Ex vivo analysis of tracer deposition and correlation to lymphatic drainage

On average, the dorsal regions (Q2 and Q3) were shown to contain a larger fraction of the tracer deposits when compared with the ventral regions (Q1 and Q4), 71% and 29% respectively ($p < 0.001$; Wilcoxon signed-rank test, Fig. 3a). Overall, the tracer deposition was equally divided between the left (Q3–4) and the right side (Q1–2) of the prostate (50% and 50% respectively, $p = 0.96$; the Wilcoxon signed-rank test) and slightly more tracer was injected into the apex compared with the base of the prostate (43% and 57% respectively, $p = 0.003$; the Wilcoxon signed-rank test).

Confinement of the analysis to the 20% of patients with the most unequally balanced tracer deposition between right and left side of the prostate (the 7 patients with most tracer deposition to the left and the 7 patients with the most tracer deposition to the right were selected), provided a significant correlation between the site of tracer deposition site and the lateralized drainage pattern (r, 0.81; $p < 0.001$; Pearson correlation) (Fig. 3b). In the group wherein tracer deposition was located mostly to the left, on average 4.0 LNs (IQR, 2-5.5; 3.0 to the left; 1.0 to the right) were visualized and in the group wherein tracer deposition was located mostly to the right side on average 3.6 LNs (IQR, 3–4, 1.1 to the left, 2.4 to the right) were identified.

To help understand how the effect of tracer deposition in the dorsal half of the prostate related to the tracer deposition in the ventral half of the prostate, the 7 patients with the most dorsal tracer deposition and the 7 patients with the most ventral tracer deposition were selected. On average 3.7 LNs (IQR, 2–4; 2.7 to the left; 1.7 to the right) were visualized in the patients with the most dorsal tracer deposition and on average 2.3 LNs (IQR, 1–3; 1.3 to the left, 1.0 to the right) were visualized in the patients with the most ventral tracer deposition. There seemed to be a hint towards a negative effect of tracer deposition in the ventral half of the prostate on the number of draining LNs, but this finding was not significant ($p = 0.39$; the Mann Whitney U test, Fig. 3c).

Assessment of the tracer distribution between the base and apex revealed that these anatomical locations resulted in different drainage patterns. Instead of confinement to the 20% of patients with the most unequal tracer deposition, only the patients with the most equal tracer deposition (40%–60% tracer deposition in apex or base; 24 patients) were excluded from the total cohort. The lymphatic drainage pattern of patients with ≥ 60% tracer deposition near the base was compared with the lymphatic drainage pattern of ≥ 60% tracer deposition in the apex as quantified by post-operatively imaging of the paraffin-embedded prostate tissue blocks. In both these groups LN visualization was equally divided between the right and left side of the body ($p_{base} = 0.132$, $p_{apex} = 0.623$; the Wilcoxon signed-rank test). In the group of patients with ≥ 60% tracer deposition in the base, mainly LNs were visualized in the obturator fossa (50%) and the external iliac (32%) region, while in the group of patients with ≥ 60% tracer deposition in the apex, mainly LNs were visualized in the obturator fossa (37%) and internal iliac (25%) region. Interestingly, most of the LNs visualized and dissected in the pre-prostatic region (90%) occurred in the group of patients with ≥ 60% tracer deposition in the apex (Fig. 3d).

Relation between the location of the primary tumour and the location of nodal metastases

Overall, histopathologic analysis of the excised lymphatic tissue (ePLND and SN specimens combined) yielded 764 LNs, of which 32% was tracer-positive and 68% was tracer-negative. In the ten LN metastases bearing patients (15%), a total of 38 tumour-positive LNs were found, of which 20 were tracer-positive (53%) and 18 tracer-negative (47%). In six patients (60% of all pN1 patients), the tracer-positive SNs were the only tumour-bearing nodes. In three other patients, both tracer-positive SNs and tracer-negative tumour-bearing LNs were found. In one patient, two SNs outside of the ePLND field contained nodal metastases (false negative ePLND case). In another patient, the tumour-bearing LN showed no tracer uptake, resulting in a false negative SN case.

The primary tumour distribution in the excised prostate tissue of the ten patients with the tumour-bearing LNs was histopathological analysed (Fig. 4a). The relative tumour surface was equally distributed between the left (Q3, 4) and the right side (Q1, 2) of the prostate, 49% and 51% respectively ($p = 0{,}878$; the Wilcoxon signed-rank test). Tumour was more prevalent in the dorsal half (Q2, 3) compared to the ventral

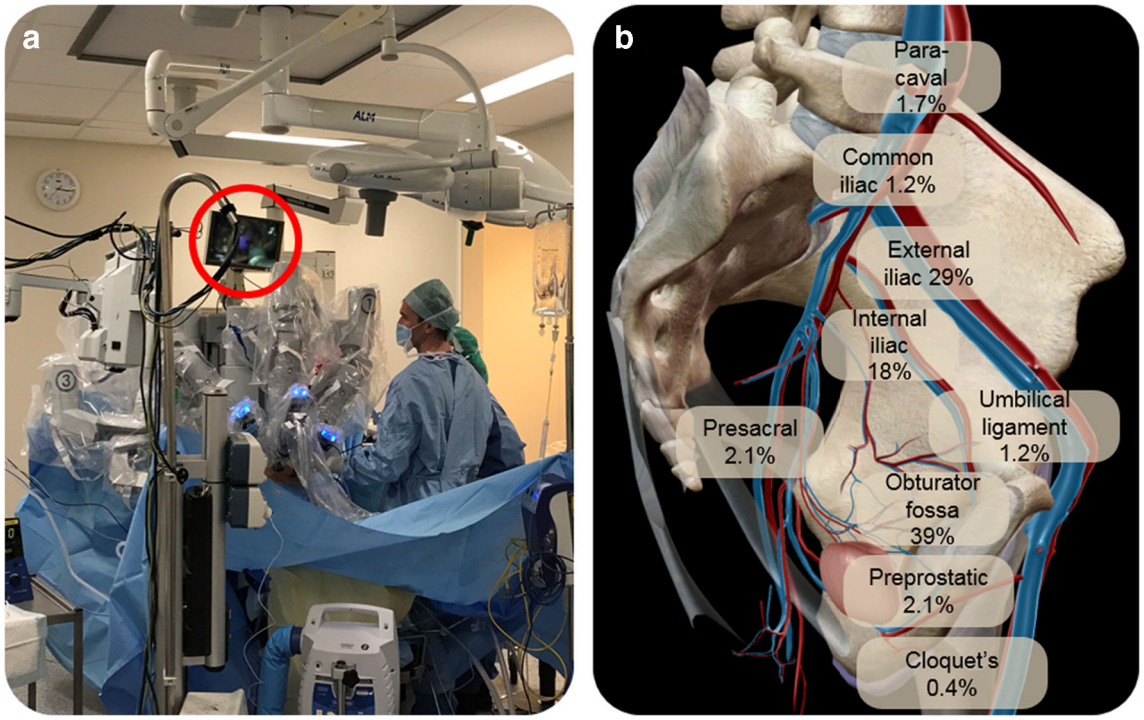

Fig. 2 Intraoperative identification of LNs. **a** During the surgical procedure, the SNs were identified using the fluorescence signal of ^{99m}Tc-nanocolloid (red circle). **b** An overview of the locations of the visualized and dissected SNs, the location of 5.4% of the SNs was undetermined

half of the prostate (Q1, 4), 68% and 32% respectively (p = 0,074; the Wilcoxon signed-rank test). Intraprostatic tumour spread was equally divided over the base and the apex, 56% and 44% respectively (p = 0,284; the Wilcoxon signed-rank test) (Fig. 4b).

For each of the three orientations (left vs. right, dorsal vs. ventral, base vs. apex), the distribution of the tumour-bearing LNs seemed to be related to the primary tumour distribution in the same way as the lymphatic drainage pattern was correlated to the tracer deposition. For 97% of the tumour-bearing LNs, at least 25% of the primary tumour content was found at the same side of the tumour-bearing LNs (Fig. 5a). In 7/10 of the patients with tumour-bearing LNs, the dorsal half of the prostate contained most of the tumour burden (> 55%). In line with this, more tumour-bearing LNs were recovered from patients presenting tumour in the dorsal half compared with the patients presenting tumour in ventral half (4.6 vs. 2.0 LNs respectively) (Fig. 5b). When tumour was located in the base or the apex, the nodal metastases were more likely to be present in those nodes found to drain from the base or the apex, respectively (Fig. 3, and Fig. 5c). Taken together, these findings indicate that there is a direct relationship between the location of the primary tumour and the location of the tumour-bearing LNs similar to the relationship between tracer deposition and lymphatic drainage.

Relation between tracer deposition and the visualization of nodal metastases

Lastly, the imaging-based findings (relationship between lymphatic drainage and tracer deposition) and the pathological findings (relationship between lymphatic spread and primary tumour location) were compared for the ten patients with nodal metastases were compared. The two typical examples of this comparison presented in Fig. 6 indicate a direct relation between the imaging-based and pathological findings. The first case is an example of intratumoural tracer deposition which resulted in a true positive case (Fig. 6a). Here, the tumour was located mainly in the dorsal half at the left side of the prostate (left vs. right, 67% vs. 33%; dorsal vs. ventral, 95% vs. 5%; base vs. apex, 49% vs. 51%). The tracer was deposited to the different parts of the prostate (left vs. right, 31% vs. 69%; dorsal vs. ventral, 70% vs. 30%; base vs. apex, 37% vs. 63%). The tracer deposition resulted in lymphatic drainage to both sides of the body and in the visualization of five tumour-bearing LNs, 4 to the left, and 1 to the right. The second case is an example of ineffective extratumoural tracer deposition, which resulted in the only false negative case in our series (Fig. 6b). Here, the tumour was located mainly in the ventral half at the left side of the prostate (left vs. right, 80% vs. 20%; dorsal vs. ventral, 34% vs. 66%; base vs. apex, 49% vs. 51%). The tracer was injected into the different halves of the prostate (left vs. right, 45% vs. 55%; dorsal vs. ventral,

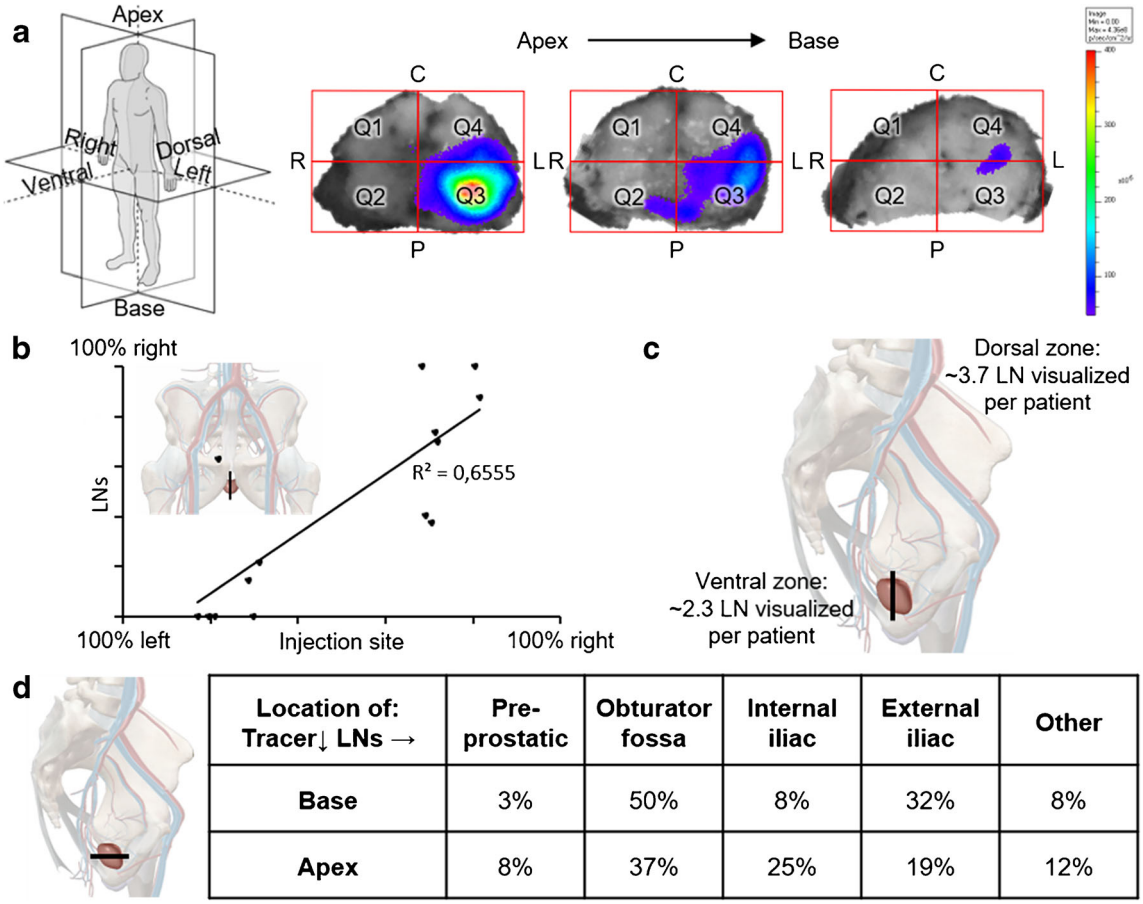

Location of: Tracer↓ LNs →	Pre-prostatic	Obturator fossa	Internal iliac	External iliac	Other
Base	3%	50%	8%	32%	8%
Apex	8%	37%	25%	19%	12%

Fig. 3 Effect of tracer deposition on lymphatic mapping. **a** The tracer deposition was quantified postoperatively for every tissue block per quartile (Q1–4) based on the fluorescence signal from the tracer (coloured hotspots). **b** The location of the LNs visualized using lymphoscintigraphy (left vs. right) was plotted against the location of the injection site (left (Q3–4) vs. right (Q1–2)) for 20% of the patients with the most unequal tracer deposition within in the prostate. **c** The number of visualized LNs found after more dorsal vs ventral tracer deposition. **d** The lymphatic drainage pattern caused by ≥60% tracer injection into the base or the apex

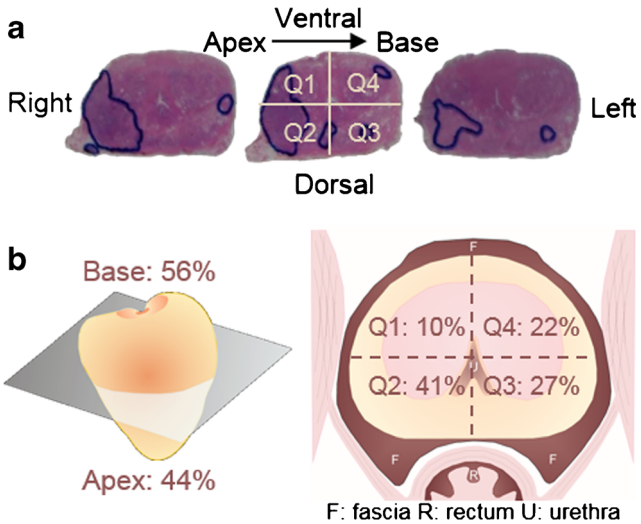

Fig. 4 Primary tumour distribution throughout the prostate. **a** The surface of the prostate and the surface of the tumour (blue line) was determined based on the pathological evaluation of HE stained tissue slides. **b** The distribution of the tumour location (calculated based on HE stained prostate sections using a MATLAB script)

76% vs. 24%; base vs. apex, 53% vs. 47%), mostly outside the tumour. Subsequently, lymphatic tracer drainage was only seen to the right side of the body, while pathology revealed a metastasis on the left side of the body.

Discussion

Besides providing image guidance, exploration of the fluorescent, and radioactive properties of the hybrid tracer ICG-^{99m}Tc-nanocolloid has allowed a direct relation to be made between the lymphatic drainage process and the metastatic dissemination route from the primary tumour sites. Combined, these data show that intraprostatic tracer deposition at the location of the primary tumour site(s) is important for identification of LN metastases via tracer guided nodal dissection.

In line with the SN concept, tracer deposition is directly related to the primary tumour site in most indications where SN procedures are performed [24]. Key examples hereof are

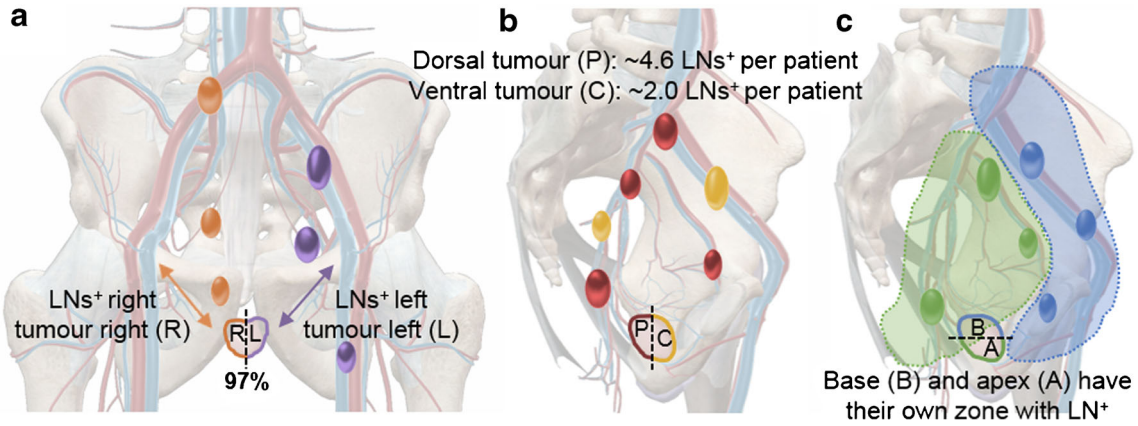

Fig. 5 Tumour location and tumour bearing LN location. **a** Relationship between location of the tumour bearing LNs (LNs^+) and the primary tumour location; right (R; orange) vs. left (L; purple). **b** Relationship between the number of visualized tumour bearing LNs (LNs^+) and the primary tumour location; dorsal (P; red) half vs. ventral (C; yellow) half. **c** Relationship between location of the tumour bearing LNs (LNs^+) and the primary tumour location; apex (A; green) vs. base (B; blue)

melanoma, oral cavity, and (part of the) breast tumours [25–27]. For practical reasons, in some instances, the organ rather than the tumour is targeted in patients with breast, penis, testis, or prostate cancer [28–31]. This may be suboptimal and result in a false negative SNB. Indeed, a study in multifocal breast cancer patients [32] revealed that individual tumours in the same organ can present different drainage patterns. As technical optimizations of SN procedures in the form of tracers and hardware have already been studied extensively [17, 22], investigation of the impact of the tracer deposition site on the visualized lymphatic drainage pattern provides a logical next step in the technical refinement of the SN procedures.

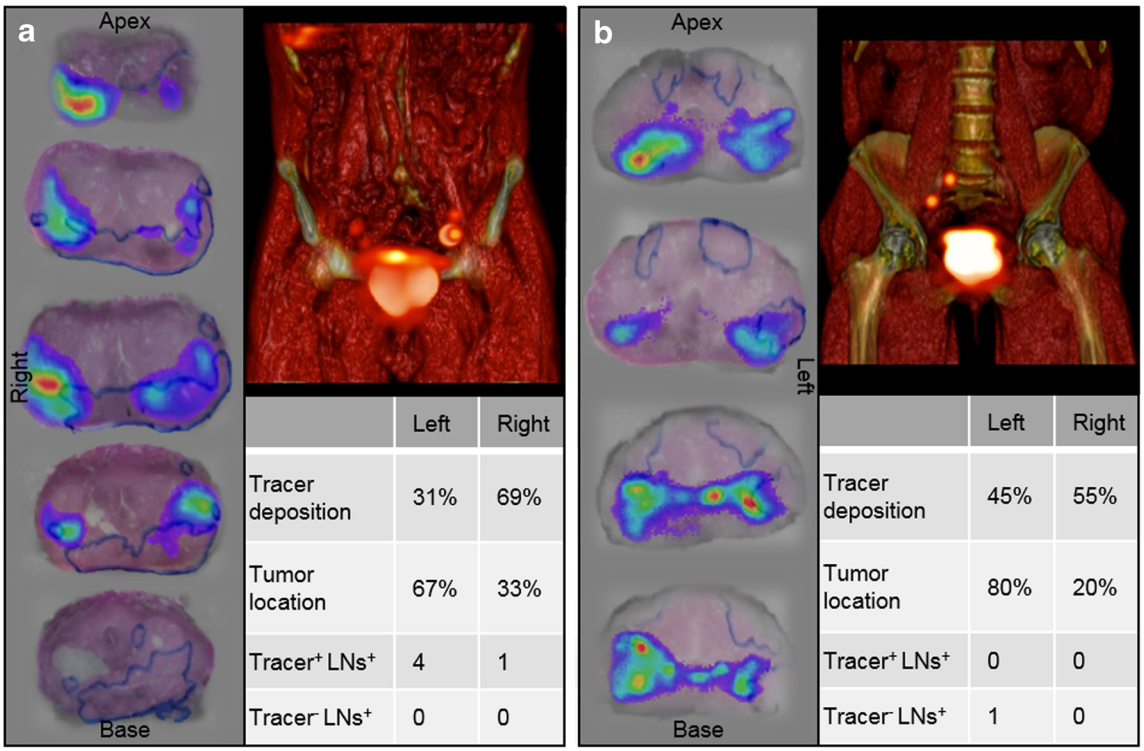

Fig. 6 The effect of tracer deposition on the lymphatic drainage pattern. **a** Example of a correct intratumoural tracer deposition (case 1): The overlay of the HE stained tissue slides with the fluorescence measurements of the tracer deposition is shown, together with the corresponding SPECT image and the distribution of the tracer deposition and tumour location and the numbers of visualized and non-visualized tumour bearing LNs are listed ($Tracer^+$ LNs^+ and $Tracer^-$ LNs^+). **b** Example of an ineffective extratumoural tracer deposition (case 2): The overlay of the HE stained tissue slides with the fluorescence measurements of the tracer deposition is shown, together with the corresponding SPECT image, the distribution of the tracer deposition, tumour location and the numbers of visualized and non-visualized tumour bearing LNs are listed

In accordance with previous studies, intratumoural injections are relevant for SN identification in PCa. First, PCa is heterogeneously distributed through the organ so different primary tumour sites may have different lymphatic dissemination paths [33]. Second, the prostate consists of three anatomically distinctly different glandular regions which could again constitute different lymphatic drainage [34, 35]. The impact of the tracer deposition site on the lymphatic drainage was studied by considering three different orientations (left vs. right, dorsal vs. ventral and base vs. apex). These three comparisons did indeed revealed that the location of the tracer deposits in the prostate affects the observed lymphatic tracer drainage patterns. The findings of this study (see also Fig. 6), also specifically indicate that intratumoural tracer deposition increases the chance of identifying metastases containing LNs compared with cases were tracer deposition occurred outside the tumour. In fact, the only false negative SNB case was a patient were the tracer deposition and resulting lymphatic did not match with the tumour distribution.

In surgical guidance, different modalities support different types of diagnostics. The diagnostic possibilities offered by the use of a tracer with a radioactive and a fluorescent label were shown to both be required to enable nodal staging and intraoperative SN identification. Where radioisotopes decay over time ($t_{1/2}$ = 6 h for ^{99m}Tc), fluorescence signals like those of ICG—when specimens are kept in the dark—remain visible in pathological specimens long after their excision. In this case, even longer than 5 years. This concept has proven its worth with tumour receptor-targeted fluorescence tracers [36, 37] and has also proven value with hybrid tracers [38, 39]. In case of the hybrid tracer ICG-^{99m}Tc-nanocolloid, the partial drainage from the injection site combined with the grafting of the tracer in the interstitial cell volume as result of the injection pressure enabled, as shown before [20], clear post-operative localization of the tracer using ex vivo fluorescence imaging (see Fig. 3a). It is not clear whether the same results could be achieved with "free" ICG. In contrast to ICG coupled to ^{99m}Tc-nanocolloid, "free" ICG binds to plasma proteins and since there is no clear uptake mechanism known for these proteins, they are likely to wash out during pathological sample preparation.

A limitation of the current study is the fact that it represents a retrospective analysis of the impact of the tracer deposition site, while in all patients the intent was to place four tracer deposits in the dorsal half of the prostate. Transrectal positioning of the needle to administer the tracer was performed under ultrasound guidance, which has a limited sensitivity for tumour visualization. However, MRI- and/or PET-guided ultrasound-fusion needle navigation technologies have the potential to allow precise targeting of multiple PCa sites within a single prostate [40]. These new technologies could be of value to guide tracer injection for SNB of the prostate. A randomized trial comparing intratumoural tracer deposition to intraprostatic tracer deposition is further needed to establish if our initial findings can prospectively be confirmed. Evaluation of such a randomized setup should be directly linked to this together with the evaluation of the oncological impact of the presented findings. This study (M13PSN, NL46580.031.13) is currently being performed.

Conclusion

The observed relationship between the location of the tracer deposits, the location of the primary tumour, and the visualization of the (tumour-positive) SNs indicates that placement of SN tracer deposits prior to SNB of the prostate affects the correct visualization of lymphatic drainage pattern. Furthermore, intratumoural SN tracer injection could further improve the accuracy SNB accuracy.

Acknowledgements The authors would like to thank all participating patients, the entire surgical staff, and the departments of pathology and nuclear medicine of the Netherlands Cancer Institute-Antoni van Leeuwenhoek Hospital for their contribution. The authors would also like to thank Nynke van den Berg for her help to archive the findings in the database.

Funding This research was supported by an NWO-STW-VIDI grant (STW BGT 11271) and a NWO-TTW-VICI grant (TTW 16141).

Compliance with ethical standards

Conflict of interest The authors declare that they have no conflict of interest.

Ethical approval All procedures performed in this study were in accordance with the ethical standards of the local ethics committee of The Netherlands Cancer Institute - Antoni van Leeuwenhoek Hospital (N09IGF; NL28143.031.09) and with the 1964 Helsinki declaration and its later amendments or comparable ethical standards.

References

1. van Leeuwen PJ, Emmett L, Ho B, Delprado W, Ting F, Nguyen Q, et al. Prospective evaluation of 68gallium-prostate-specific membrane antigen positron emission tomography/computed tomography for preoperative lymph node staging in prostate cancer. BJU Int. 2017;119(2):209–15.
2. Maurer T, Gschwend JE, Rauscher I, Souvatzoglou M, Haller B, Weirich G, et al. Diagnostic efficacy of (68)gallium-PSMA positron emission tomography compared to conventional imaging for lymph node staging of 130 consecutive patients with intermediate to high risk prostate cancer. J Urol. 2016;195(5):1436–43.
3. Kim SJ, Lee SW, Ha HK. Diagnostic performance of radiolabeled prostate-specific membrane antigen positron emission tomography/computed tomography for primary lymph node staging in newly diagnosed intermediate to high-risk prostate cancer patients: a systematic review and meta-analysis. Urol Int. 2019;102(1):27–36.
4. Mottet N, Bellmunt J, Bolla M, Briers E, Cumberbatch MG, De Santis M, et al. EAU-ESTRO-SIOG guidelines on prostate cancer.

Part 1: screening, diagnosis, and local treatment with curative intent. Eur Urol. 2017;71:618–29.
5. Briganti A, Chun FK, Salonia A, Suardi N, Gallina A, Da Pozzo LF, et al. Complications and other surgical outcomes associated with extended pelvic lymphadenectomy in men with localized prostate cancer. Eur Urol. 2006;50(5):1006–13.
6. van Leeuwen FWB, Winter A, van Der Poel HG, Eiber M, Suardi N, Graefen M, et al. Technologies for image-guided surgery for managing lymphatic metastases in prostate cancer. Nat Rev Urol. 2019;16(3):159–71.
7. Weckermann D, Dorn R, Trefz M, Wagner T, Wawroschek F, Harzmann R. Sentinel lymph node dissection for prostate cancer: experience with more than 1,000 patients. J Urol. 2007;177(3): 916–20.
8. Weckermann D, Dorn R, Holl G, Wagner T, Harzmann R. Limitations of radioguided surgery in high-risk prostate cancer. Eur Urol. 2007;51(6):1549–56 discussion 56-8.
9. Joniau S, Van den Bergh L, Lerut E, Deroose CM, Haustermans K, Oyen R, et al. Mapping of pelvic lymph node metastases in prostate cancer. Eur Urol. 2013;63(3):450–8.
10. Roscigno M, Nicolai M, La Croce G, Pellucchi F, Scarcello M, Sacca A, et al. Difference in frequency and distribution of nodal metastases between intermediate and high risk prostate cancer patients: results of a superextended pelvic lymph node dissection. Front Surg. 2018;5:52.
11. Mattei A, Fuechsel FG, Bhatta Dhar N, Warncke SH, Thalmann GN, Krause T, et al. The template of the primary lymphatic landing sites of the prostate should be revisited: results of a multimodality mapping study. Eur Urol. 2008;53(1):118–25.
12. van den Berg NS, Valdes-Olmos RA, van der Poel HG, van Leeuwen FW. Sentinel lymph node biopsy for prostate cancer: a hybrid approach. J Nucl Med. 2013;54(4):493–6.
13. Winter A, Woenkhaus J, Wawroschek F. A novel method for intraoperative sentinel lymph node detection in prostate cancer patients using superparamagnetic iron oxide nanoparticles and a handheld magnetometer: the initial clinical experience. Ann Surg Oncol. 2014;21(13):4390–6.
14. Manny TB, Patel M, Hemal AK. Fluorescence-enhanced robotic radical prostatectomy using real-time lymphangiography and tissue marking with percutaneous injection of unconjugated indocyanine green: the initial clinical experience in 50 patients. Eur Urol. 2014;65(6):1162–8.
15. Jeschke S, Lusuardi L, Myatt A, Hruby S, Pirich C, Janetschek G. Visualisation of the lymph node pathway in real time by laparoscopic radioisotope- and fluorescence-guided sentinel lymph node dissection in prostate cancer staging. Urology. 2012;80(5):1080–6.
16. van den Berg NS, Buckle T, KleinJan GH, van der Poel HG, van Leeuwen FW. Multispectral fluorescence imaging during robot-assisted laparoscopic sentinel node biopsy: a first step towards a fluorescence-based anatomic roadmap. Eur Urol. 2016;72(1):110–7.
17. KleinJan GH, van Werkhoven E, van den Berg NS, Karakullukcu MB, Zijlmans H, van der Hage JA, et al. The best of both worlds: a hybrid approach for optimal pre- and intraoperative identification of sentinel lymph nodes. Eur J Nucl Med Mol Imaging. 2018;45(11): 1915–25.
18. van der Poel HG, Buckle T, Brouwer OR, Valdes Olmos RA, van Leeuwen FW. Intraoperative laparoscopic fluorescence guidance to the sentinel lymph node in prostate cancer patients: clinical proof of concept of an integrated functional imaging approach using a multimodal tracer. Eur Urol. 2011;60(4):826–33.
19. Brouwer OR, van den Berg NS, Matheron HM, van der Poel HG, van Rhijn BW, Bex A, et al. A hybrid radioactive and fluorescent tracer for sentinel node biopsy in penile carcinoma as a potential replacement for blue dye. Eur Urol. 2014;65(3):600–9.
20. Buckle T, Brouwer OR, Valdes Olmos RA, van der Poel HG, van Leeuwen FW. Relationship between intraprostatic tracer deposits and sentinel lymph node mapping in prostate cancer patients. J Nucl Med. 2012;53(7):1026–33.
21. Pano B, Sebastia C, Bunesch L, Mestres J, Salvador R, Macias NG, et al. Pathways of lymphatic spread in male urogenital pelvic malignancies. Radiographics. 2011;31(1):135–60.
22. KleinJan GH, van den Berg NS, Brouwer OR, de Jong J, Acar C, Wit EM, et al. Optimisation of fluorescence guidance during robot-assisted laparoscopic sentinel node biopsy for prostate cancer. Eur Urol. 2014;66:991–8.
23. Nieweg OE, Tanis PJ, Kroon BB. The definition of a sentinel node. Ann Surg Oncol. 2001;8(6):538–41.
24. Morton DL, Wen DR, Wong JH, Economou JS, Cagle LA, Storm FK, et al. Technical details of intraoperative lymphatic mapping for early stage melanoma. Arch Surg. 1992;127(4):392–9.
25. Rettenbacher L, Koller J, Kassmann H, Holzmannhofer J, Rettenbacher T, Galvan G. Reproducibility of lymphoscintigraphy in cutaneous melanoma: can we accurately detect the sentinel lymph node by expanding the tracer injection distance from the tumor site? J Nucl Med. 2001;42(3):424–9.
26. Tartaglione G, Stoeckli SJ, de Bree R, Schilling C, Flach GB, Bakholdt V, et al. Sentinel node in oral cancer: the nuclear medicine aspects. A survey from the sentinel European node trial. Clin Nucl Med. 2016;41(7):534–42.
27. Weber JJ, Wong JH. Periareolar or peritumoral injection of isosulfan blue and the effect on the number of sentinel lymph nodes examined. Am Surg. 2017;83(1):98–102.
28. Cong BB, Cao XS, Qiu PF, Liu YB, Zhao T, Chen P, et al. Validation study of the modified injection technique for internal mammary sentinel lymph node biopsy in breast cancer. Onco Targets Ther. 2015;8:2705–8.
29. Lutzen U, Zuhayra M, Marx M, Zhao Y, Knupfer S, Colberg C, et al. Value and efficacy of sentinel lymph node diagnostics in patients with penile carcinoma with nonpalpable inguinal lymph nodes: five-year follow-up. Clin Nucl Med. 2016;41(8):621–5.
30. Blok JM, Kerst JM, Vegt E, Brouwer OR, Meijer RP, Bosch J, et al. Sentinel node biopsy in clinical stage I testicular cancer enables early detection of occult metastatic disease. BJU Int. 2018. https://doi.org/10.1111/bju.14618.
31. van der Poel HG, Meershoek P, Grivas N, KleinJan G, van Leeuwen FW, Horenblas S. Sentinel node biopsy and lymphatic mapping in penile and prostate cancer. Urologe A. 2017;56(1):13–7.
32. Brouwer OR, Vermeeren L, van der Ploeg IM, Valdes Olmos RA, Loo CE, Pereira-Bouda LM, et al. Lymphoscintigraphy and SPECT/CT in multicentric and multifocal breast cancer: does each tumour have a separate drainage pattern? Results of a Dutch multicentre study (MULTISENT). Eur J Nucl Med Mol Imaging. 2012;39(7):1137–43.
33. Lovf M, Zhao S, Axcrona U, Johannessen B, Bakken AC, Carm KT, et al. Multifocal primary prostate cancer exhibits high degree of genomic heterogeneity. Eur Urol. 2019;75(3):498–505.
34. McNeal JE. Anatomy of the prostate and morphogenesis of BPH. Prog Clin Biol Res. 1984;145:27–53.
35. Brossner C, Ringhofer H, Hernady T, Kuber W, Madersbacher S, Pycha A. Lymphatic drainage of prostatic transition and peripheral zones visualized on a three-dimensional workstation. Urology. 2001;57(2):389–93.
36. Burggraaf J, Kamerling IM, Gordon PB, Schrier L, de Kam ML, Kales AJ, et al. Detection of colorectal polyps in humans using an intravenously administered fluorescent peptide targeted against c-Met. Nat Med. 2015;21(8):955–61.
37. Dobosz M, Haupt U, Scheuer W. Improved decision making for prioritizing tumor targeting antibodies in human xenografts: utility of fluorescence imaging to verify tumor target expression, antibody

binding and optimization of dosage and application schedule. MAbs. 2017;9(1):140–53.
38. Buckle T, Kuil J, van den Berg NS, Bunschoten A, Lamb HJ, Yuan H, et al. Use of a single hybrid imaging agent for integration of target validation with in vivo and ex vivo imaging of mouse tumor lesions resembling human DCIS. PLoS One. 2013;8(1):e48324.
39. Schottelius M, Wurzer A, Wissmiller K, Beck R, Koch M, Gorpas D, et al. Synthesis and preclinical characterization of the PSMA-targeted hybrid tracer PSMA-I&F for nuclear and fluorescence imaging of prostate cancer. J Nucl Med. 2019;60(1):71–8.
40. van Oosterom MN, van der Poel HG, Navab N, van de Velde CJH, van Leeuwen FWB. Computer-assisted surgery: virtual- and augmented-reality displays for navigation during urological interventions. Curr Opin Urol. 2018;28(2):205–13.